Changing water availability and demand shift global greening to regional browning

Rene Orth

rene.orth@ecoclim.uni-freiburg.de

University of Freiburg

Jasper Denissen

ECMWF

Josephin Kroll

University of Freiburg

Sungmin O

Kangwon National University https://orcid.org/0000-0002-7364-2122

Ana Bastos

Max Planck Institute for Biogeochemistry (MPI-BGC), Germany https://orcid.org/0000-0002-7368-7806

Wantong Li

Max Planck Institute for Biogeochemistry https://orcid.org/0000-0001-9861-4294

Diego Miralles

Ghent University https://orcid.org/0000-0001-6186-5751

Melissa Ruiz-Vasquez

Max Planck Institute for Biogeochemistry https://orcid.org/0000-0001-9847-3399

Anne Hoek van Dijke

Max Planck Institute for Biogeochemistry

Andrew Feldman

NASA Goddard Space Flight Center

Mirco Migliavacca

European Commission Joint Research Center (JRC), Bioeconomy and Forests D.1 Unit https://orcid.org/0000-0003-3546-8407

Lan Wang-Erlandsson

Stockholm University https://orcid.org/0000-0002-7739-5069

Benjamin Stocker

University of Bern

Adriaan J. Teuling

Wageningen University & Research https://orcid.org/0000-0003-4302-2835

Hui Yang

Peking University
Chunhui Zhan
Max Planck Institute for Biogeochemistry
Xin Yu
Max Plnack Institute for Biogeochemistry

Article

Keywords:

Posted Date: December 13th, 2024

DOI: https://doi.org/10.21203/rs.3.rs-5537189/v1

Additional Declarations: There is **NO** Competing Interest.

Abstract

The Earth is greening in many regions due to increased temperature, higher atmospheric CO_2 concentration, and land use change. However, while climate change has been accelerating, greening has not kept pace in many regions. Here, we show that decreasing water availability and increasing atmospheric water demand are regionally coinciding with browning trends over recent decades. In affected tropical regions, a regression analysis considering a comprehensive set of hydro-meteorological variables confirms that both water availability and atmospheric water demand are dominant drivers of inter-annual variability in Leaf Area Index (LAI). Earth system models mostly reproduce the observed spatial extent of browning and related coinciding water changes in the multi-model mean, while simulations from individual models differ strongly. Our results provide a new constraint for related model development and underscore the need for enhanced monitoring and consideration of observation-based water availability trends as an emerging driver of vegetation in future analyses and model development.

Introduction

Terrestrial vegetation provides essential ecosystem and climate services such as food supply, carbon storage, and evaporative cooling (Bonan et al. 2008), and contributes to the uptake of about one third of anthropogenic CO_2 emissions (Gulev et al. 2021, Friedlingstein et al. 2022). Furthermore, vegetation can mediate land surface responses to extreme events such as heat waves (Forzieri et al. 2017, Forzieri et al. 2020), droughts, floods (Ukkola et al. 2016, Hoek van Dijke et al. 2022), and fires (O et al. 2020) through its impacts on evaporative cooling (Seneviratne et al. 2010), runoff (W. Li et al. 2023), cloud formation (Xu et al. 2022), and precipitation (Smith et al. 2023).

A greening of the Earth's land surface has been observed since the 1980s in many areas across the globe (Donohue et al. 2013, Zhu et al. 2016, Chen et al. 2019, Winkler et al. 2021). The greening has been attributed to increasing temperature, rising atmospheric CO_2 concentration (Donohue et al. 2013, Zhu et al. 2016, Winkler et al. 2021) and nitrogen deposition (Zhu et al. 2016), as well as to human land-use changes and management, e.g. fertilization, irrigation or revegetation (Chen et al. 2019, Ruijsch et al. 2023). The relevance of these drivers varies spatially, where temperature increases are most relevant in high-latitude regions while management has contributed to greenness trends in south-east Asia (Chen et al., 2019). The greening, in turn, has contributed to changes in ecosystem functioning such as increased transpiration and associated evaporative cooling (Forzieri et al. 2020, Zhan et al. 2022, Yang et al. 2023), and likely also to the land sink of anthropogenic carbon (Ruehr et al. 2023).

Next to energy (e.g. temperature, radiation) and nutrients (e.g. nitrogen) (Piao et al. 2019, Denissen et al. 2020), water is an essential prerequisite for vegetation functioning. Water consumption through transpiration is directly linked to CO_2 assimilation via diffusion through stomatal openings. While temperature and CO_2 concentration have continued to this increase (Gonsamo et al. 2021, Gulev et al. 2021), there is considerable uncertainty on whether this will continue translating into greening (Jiang et al. 2017, Piao et al. 2020, Frankenberg et al. 2021, Winkler et al. 2021) and evidence is mounting for

increasing episodic and local browning which slows down the global greening trend (Feng et al. 2021, Q. Liu et al. 2023).

Past studies on vegetation greening trends and its drivers have either not separated the effects of vegetation water limitation or found it to be a minor control (Chen et al. 2019, Winkler et al. 2021). Also, in some of these cases, the overall climate change effect is considered without explicitly distinguishing the role of water limitation from that of e.g. warming. Studies based on dynamic vegetation models intrinsically account for water limitation; however, water limitation is not accurately represented in many models (Gentine et al. 2019, W. Li et al. 2023). An increasing importance of vegetation water limitation on greenness was shown in Feng et al. (2021) and Jiao et al. (2021), while the latter particularly highlights the role of droughts. More recent studies find an increasing sensitivity of vegetation to soil moisture in many regions across the world, both in recent decades and future projections (Denissen et al. 2022, Li et al. 2022). This increase in the vegetation's sensitivity to water might reflect an increase in water-limited conditions in response to a changing climate. Decreasing soil moisture and increasing vapor pressure deficit are projected in many regions (Gulev et al. 2021). Water stress can slow down vegetation greening trends by (i) introducing episodic browning where hydraulic vulnerability thresholds are exceeded during days or weeks and the tissue is irreversibly damaged; at the same time (ii) there could also be more gradual changes in LAI by which tree architecture acclimates in response to decadal trends in atmospheric water demand, plant water use efficiency, and water availability. While research focuses considerably on vegetation greening, the influence of trends in water availability and demand remains uncertain and often not explicitly addressed in most greening-related studies. Only 39% of the greening-related publications in 2022 in the Web of Science relate specifically to water or moisture (search terms "vegetation", "greening", and "water" or "moisture").

Water availability and atmospheric water demand for vegetation can be represented in different ways using single variables such as soil moisture, vapor pressure deficit, precipitation and water potential, or combined indices such as aridity index, precipitation minus evaporation, and Palmer Drought Severity Index. Studies on respective trends yield partly contrasting results (Huang et al. 2016, Vicente-Serrano et al. 2022a, Z. Liu et al. 2023), probably because the employed indices differ in their consideration of water supply and/or atmospheric water demand. In fact, plant functioning is affected by different water-related variables through different pathways. Plants absorb water mainly from the soil through their roots, when soil moisture content is above the wilting point such that water is accessible. This water moves through the xylem of the plant and is released through the stomata on the bottom of the leaves by transpiration. When soils are dry or atmospheric water demand is high, plants can (partly) close the stomata to minimize the water loss (Novick et al. 2016, Fu et al. 2022). This prevents hydraulic failure, i.e., cavitation in the xylem which inhibits the water transport, while at the same time it leads to reduced CO_2 assimilation and consequently potentially reduced vegetation growth.

Main text

In this study, we compare global patterns of trends in vegetation greenness with those in water availability and atmospheric water demand. We use leaf area index (LAI) as an indicator of vegetation greenness. We quantify the trends in annual-mean LAI and water-related variables, and contrast them between the recent past (2002–2020) and the preceding period (1982–2001) in order to detect potential changes in those trends. Acknowledging the relevance of multiple water-related variables, we use a suite of these variables here including soil moisture, precipitation, dryness index, and vapor pressure deficit (VPD) (see Methods). VPD can decrease vegetation productivity even if soil moisture is not limiting (Fu et al. 2022). In particular, we analyse the agreement of trends across these variables with respect to decreased water availability or increased water demand (see Methods for details). To further determine the relevance of water availability and demand for inter-annual LAI dynamics, we perform a regression-based driver attribution analysis at each grid cell where a range of energy- and water-related variables are considered as potential drivers (see Methods). We consider annual averages of the water- and energy-related variables, and additionally we use monthly soil moisture minima and daily temperature maxima per year to represent droughts and heat waves. This allows us to compare the impact of gradual changes in hydro-meteorological variables on vegetation greenness with that of hydro-meteorological extremes.

The analyses are performed with both observation-based data and Earth system model output. Observation-based data include hydro-meteorological variables from various independent datasets (see Methods), and LAI data from the GEOV2 and MODIS datasets (Verger et al. 2020) (see Methods for details). In addition, we consider historical and SSP5-8.5 scenario simulations from nine Earth system models from the sixth phase of the coupled model intercomparison project (CMIP6) which provide all variables required for our analysis (see Methods for details).

Global trends in LAI and water-related variables

Figure 1a,b shows evidence for widespread global greening during 1982–2001, particularly in the northern mid and high latitudes and the tropics, which then slows down during 2002–2020 with regionalized browning in addition to continued greening in other regions. The browning emerges mostly in tropical regions such as the eastern Amazon and western central Africa as well as in high latitudes across parts of Canada, Alaska and eastern Siberia. Note that for the earlier period 1982–2001, LAI data can only be inferred from observations from the Advanced Very High-Resolution Radiometer (AVHRR). This data suffers from temporal inconsistency caused by inconsistent biases with ground reference stations and satellite orbital drift, which induces uncertainty in the long-term trends of LAI inferred from AVHRR observations (Zhu et al. 2016, Jiang et al. 2017, Jeong et al. 2024). The GEOV2 product employed here aims to compensate for inconsistencies in the AVHRR data, and the results are largely consistent with independent LAI data from MODIS (Figure S1). We note that while, different state-of-the-art LAI products still disagree in the strength of the slowdown of global greening (Jeong et al. 2024), here we focus on evaluating the role of drying for these trends.

Next, we analyse the agreement of trends across four water-related variables that represent decreased water availability and/or increased water demand. The resulting drying hot-spot regions are shown in Fig. 1c,d. In both time windows, a drying trend was observed for approx. 4% of the global study area, however, the regions with strong drying vary over time. During 1982–2001, drying is most pronounced south of the Amazon, in eastern tropical Africa and in north-eastern Europe. Thereafter, during 2002–2020 these regions do not show continued drying while drying is found in the eastern Amazon, central tropical Africa and western Russia. Figure S2 displays the trends of the individual water-related variables. While some similarity is found between the precipitation and soil moisture trend patterns, the spatial patterns and the extent of drying mostly differ between variables and time periods. This highlights the complexity of changes in water availability and demand, which are also related to each other. Largest extent of drying regions is found for VPD and is related to increasing temperature across most of the globe allowing the air to absorb more water which consequently leads to decreasing relative humidity and increasing atmospheric water demand. This suggests that water-related variables are affecting LAI mainly through their interplay, rather than because of the dominant influence of individual variables. Note that the statistical significance of the detected trends is not only affected by the strength of the trends but also by the interannual LAI variability, where the latter differs across regions.

To investigate if drying trends potentially caused browning trends, we study whether the drying trends coincide with browning trends in Fig. 1e,f. In the first time period 1982–2001 we find hardly any regions with coinciding browning and drying. This is related to the fact that very few regions with browning are detected during this period. During 2002–2020, however, some regions with combined browning and drying emerge, mostly across the Amazon, western-central tropical Africa, and Siberia (see boxes in Fig. 1f)). While the extent of drying areas did not change much across both considered time periods, the extent of vegetation browning within those regions clearly increases from the first to the second considered time period. This could be related to the fact that in addition to the effects of increases in radiation and CO_2 promoting vegetation greenness, water-related variables are exerting increasing influence on vegetation greenness and can regionally cancel out promoting effects of other variables. At the same time, however, this result can be affected by inconsistencies in satellite data underlying the long-term LAI evolution (Jeong et al. 2024). We also analyse the relationship of the spatial patterns of the trends of the individual water variables (Figure S2) with that of LAI (Fig. 1a,b) and find weak correspondence (Cramer's V around or below 0.1 across water-related variables and time periods).

Figure 2 investigates trends in LAI and water-related variables which are simulated by nine Earth system models from the sixth phase of the coupled model intercomparison project (CMIP6). Historical simulations are used until 2015, and simulations from the SSP5-8.5 scenario (O'Neill et al. 2016) thereafter. Figure 2a,b show that models are overall showing global greening in both time periods, including the large-scale spatial pattern with most pronounced greening across the northern mid and high latitudes and less greening in tropical regions. Compared with satellite-based LAI, models simulate browning over larger regions during 1982–2001 and over smaller regions during 2002–2020. Also no individual model agrees with the observed increase in browning regions between the two considered time periods (Fig. S3 and S4). An increase in the extent of browning regions is, thus, only found in the

satellite-based LAI data and not in the modelled data. However, it remains unclear whether this indicates model shortcomings or is related to the temporal inconsistencies underlying the LAI data, or both. There are considerable differences between the results of individual models as shown in Figures S3 and S4. While greening prevails for all of them, the extent of browning as well as its spatial patterns are different between the models.

Figure 2: **Model-based trends in leaf area index (LAI) and water variables during 1982–2001 (left) and 2002–2021 (right).** Analysis is performed for each of nine Earth system models separately and the figure shows summarized results. (a,b) Trends in LAI. Coloring of each grid cell indicates the most frequently occuring trend category (significant/insignificant greening or browning) across the model ensemble. Significance trends at the 95% level are marked with asterisks (see methods). Gray colors indicate limited model data availability or low agreement between models. Black color denotes that more than one trend category is most occurring across the same number of models. (c,d) Fraction of models simulating significant drying for at least two variables. Drying is quantified through decreasing water availability or increasing water demand; variables considered are root-zone soil moisture, precipitation, vapour pressure deficit and dryness index. Analyses are restricted to grid cells with data from at least five models. All trends are determined as the difference between the two considered decades.

Trends of water availability and demand in browning regions

In a next step, we focus explicitly on browning regions and analyse the degree of drying found within these regions. Figure 3a confirms that models simulate a larger extent of significant browning during 1982–2001 compared to observations which show almost no browning. In the model-based results, drying as detected in a majority of the considered water variables is only found in a small fraction of the browning areas. This suggests that changes in water availability and demand may play a role regionally while most browning is related to other causes. The results across individual models differ greatly in terms of both the simulated extent of browning (as also seen in Figures S3 and S4) and in the simulated extent of coinciding drying. Figure 3b shows similar model-based results for the period 2002–2020 even though individual models simulate slightly different extents of browning and drying compared with the earlier time period. Further, the multi-model mean results are similar to the observation-based results for this time period with regard to the extent of browning as well as the coinciding drying. We reproduce Fig. 3 with additionally considering regions of insignificant browning (Figure S5). The results are similar in the sense that models simulate a larger browning area 1982–2001, and that there is no drying in more than half of the detected browning regions. A small difference to the previous results is that models are underestimating the observed extent of browning regions during 2002–2020.

These results indicate that the browning may be related to water availability and demand regionally, while other causes seem to prevail in most browning regions. These include human impacts through land management and land use changes (Carvalho et al. 2019, Liu et al. 2021), which can make it hard or impossible to detect actual climate impacts. Note in this context that (i) greenness can also change at longer time scales due to changes in vegetation composition as a result of natural succession and

ecological dynamics, e.g., grasses are replaced by shrubs or a young forest becomes a mature forest. And (ii) vegetation can also cope with drying trends through e.g. increased atmospheric CO_2 concentration which can contribute to enhanced intrinsic plant water use efficiency (Gonsamo et al. 2021, Zhang et al. 2022, Jiao et al. 2021, Vicente-Serrano et al. 2022b), and reducing their water limitation by structural adaptation through for example deeper roots (Fan et al. 2017, Singh et al. 2022, Stocker et al. 2023). These mechanisms tend to reduce vegetation sensitivity to water (Stocker et al. 2023); the finding that coinciding browning and drying is nevertheless increasing in some regions suggests that these changes in water-related variables are happening more rapidly than the rate at which vegetation can naturally adapt and acclimate to it.

Moreover, Fig. 3 confirms observation-based results from Fig. 1 of increased browning in observations between both considered time periods, and of increased coincidence of browning and drying. This is in line with previous studies providing evidence that vegetation sensitivity to water availability is increasing, which, however, focused on vegetation dynamics at shorter time scales and on individual water-related variables or indices. For example, Jiao et al. (2021) found an increasing area within the Northern Hemisphere extratropics where NDVI is significantly correlated with water availability as represented through the standardized precipitation-evaporation index (SPEI) and the Palmer Drought Severity Index (PDSI). Using a different methodological approach and datasets, Li et al. (2022) found an increasing trend in the global sensitivity of LAI to soil moisture during recent decades. Both studies report that temperature increases play a major role in driving the increased vegetation water sensitivity, in addition to other aspects such as decreasing precipitation, decreasing soil moisture, and changes in vegetation structure and physiology (Zhang et al. 2020). The relevance of each factor varies between regions. While the relevance of precipitation and soil moisture is straightforward, the prominent role of temperature can be explained by increased atmospheric dryness, as warmer air can hold more water.

We repeat this analysis of browning regions and their dryness trends for future time periods and the multi-model mean results are shown in Figure S6. There is no systematic trend in the extent of browning areas during this century, but drying becomes more common in the detected browning areas. Vice versa, the fraction of browning areas where no water-related variable shows drying decreases.

Drivers of inter-annual LAI dynamics

In order to further corroborate the detected coincidence of browning and drying trends, we perform a regression-based analysis to determine the roles of considered water-related and energy-related climate variables in explaining inter-annual LAI dynamics (see Methods). The results are shown in Fig. 4 (Figure S7 shows results for individual variables). The top panels show regions where water and energy-related variables are identified as most influential for LAI dynamics, respectively. Such spatial patterns with mainly water vs. energy-controlled vegetation dynamics have long been recognized (Budyko 1974) and further investigated more recently (Seneviratne et al. 2010, Forzieri et al. 2017, Papagiannopoulou et al. 2017, Denissen et al. 2020, Fu et al. 2021, Jiao et al. 2021, Feldman et al. 2022, Wang et al. 2022). Many

of these studies, however, focused solely on water availability and did not include water demand. The spatial extent of the area where water-related variables are found most relevant for LAI dynamics in Fig. 4 is increasing between both considered time periods. As shown in Figure S7, this is related to increasing areas where soil moisture, VPD and temperature are most relevant. The figure also indicates that both water availability and demand are relevant for LAI dynamics globally. But spatial patterns are rather noisy which could indicate the underlying relevance of spatially heterogeneous patterns of soil and vegetation types. Finally, in this analysis we also analyse the relevance of soil moisture droughts and heat waves and the results suggest these extremes are less relevant than annual average energy and water conditions. This can be related to the fact that extremes are relevant in years with particularly significant temperature maxima or soil moisture minima, but not when considering them in all years.

The lower panels in Fig. 4 show the inferred rank of the most relevant water-related variable in explaining LAI dynamics. Also in regions where energy-related variables are most relevant, water variables can additionally play a role. In the eastern Amazon and in western tropical Africa where we identified coinciding browning and drying (Fig. 1f), water-related variables are found to be most relevant in explaining LAI dynamics, while energy-related variables dominate for the Siberian region identified previously. This way, these results serve as additional evidence of the regional role of drying for inducing vegetation browning in tropical regions. Note, however, that the trends analysed in Figs. 1–3 and the results here are not fully comparable as they are based on slightly different time scales (decadal vs. annual). Note also that while our approach to determine the most relevant variable for LAI dynamics is illustrative, in reality also additional variables play a role. The response of vegetation to concurrent changes in water availability, other climate drivers, and changing CO_2 concentrations is complex (Brodribb et al. 2020, Walker et al. 2021, Zhan et al. 2022). For example, increasing CO_2 concentrations can enhance photosynthesis and/or water use efficiency which can consequently affect LAI dynamics. Thereby, the effect of different drivers can also amplify or compensate for each other (De Kauwe et al. 2021, Z. Liu et al. 2023). Also variables can interact with each other such that for example reduced water availability at the land surface can lead to reduced evaporation, which can, in turn, yield increased VPD which makes it more likely to be detected as a main driver of LAI dynamics (Novick et al. 2016, Fu et al. 2022).

In addition to annual means of water and energy-related variables, the regression analysis also includes annual soil moisture minima as a proxy for drought and annual temperature maxima as a proxy for heat waves. Figure S7 shows that while these extremes are not most relevant for LAI dynamics across widespread regions, they matter in specific locations scattered across the globe. Furthermore, the extent of regions where soil moisture droughts are most relevant increases between both considered time periods. Also previous studies have shown that hydroclimatic extremes including droughts, floods and heat waves can have profound impacts on vegetation greenness (Reichstein et al. 2013, Kroll et al. 2022) even though they did not compare the role of climate means versus that of climate extremes. Extreme event impacts can be abrupt, persistent, and difficult or impossible to reverse, due to the crossing of critical thresholds and triggering of regime shifts (Berdugo et al. 2022). The impacts of hydroclimatic

extremes on vegetation are induced through multiple biophysical and biochemical processes. For example, in the case of drought (Allen et al. 2015) (i) plants may close their stomata to save water which can lead to carbon starvation, or (ii) plants do not close their stomata to fully benefit from the surplus in available radiation, but then risk hydraulic failure (Anderegg et al. 2015, Ruehr et al. 2019). Next to such direct effects, hydroclimatic extremes also introduce cascading effects such as pathogens and insect outbreaks that cause tree mortality (Allen et al. 2015, De Brito 2021). Furthermore, droughts and heatwaves can self-propagate to neighboring regions when reduced evaporation leads to reduced precipitation and higher temperatures (Schumacher et al. 2019, Schumacher et al. 2022). More frequent extreme weather events in a warming climate (particularly droughts and heat waves, Seneviratne et al. 2021) are likely to affect trends, or to even induce abrupt and lasting shifts in vegetation greenness (He et al. 2023). This can happen as more frequent extreme events might affect the vulnerability of vegetation to future climate change (Anderegg et al. 2020, Forzieri et al. 2022).

The regression-based analysis is also applied to the Earth system model outputs. Figure 5 shows that the models overall capture the observed global pattern of the relevance of water-related variables for LAI dynamics well. Also the ranks of the relevance of water-related variables in regions where LAI dynamics are mainly controlled by energy-related variables are in good agreement with observation-based results. The area where a water-related variable is found to be most relevant is smaller than in observations. This is mainly related to an underestimated relevance of precipitation and of soil moisture droughts as shown in Figure S8. However, as Figure S8 summarizes results across models it may provide biased results for climate variables which are only relevant in small and/or scattered regions. Some individual models in Figures S9 and S10 for example show that locally, soil moisture droughts are most relevant for LAI dynamics, underlining the importance of extremes versus mean soil moisture conditions. In addition, Figures S9 and S10 illustrate that the main drivers of LAI dynamics differ greatly between models. This is probably related to different representations of the vegetation-climate coupling in general and the vegetation-water coupling in particular. Also the mechanisms through which heat waves and droughts can affect vegetation, including legacy effects, are not fully implemented in models. The models do, however, agree with observations in terms of the spatially multifaceted main controls of LAI dynamics. Simulated spatial patterns are more similar between the analysed time periods than in the case of the observed spatial patterns for both periods (Figures S7-S10).

Conclusions

In this study, we highlight the relevance of water availability and demand for vegetation greenness trends by jointly analysing a comprehensive set of climate and vegetation data streams. We show that water-related variables can regionally affect greenness trends, and should be considered in analyses of global or regional greening or browning. Our results constitute a rather conservative estimate of the relevance of water-related variables as we focus on browning areas while changes in water availability and atmospheric water demand may also slow down greening in some areas which are not (yet) browning. At the same time, soil water availability and atmospheric water demand are only two among many

relevant drivers of vegetation greenness, and our results do not question the role of other factors, such as land use change or CO_2 fertilization.

Moving beyond previous studies, we incorporate a comprehensive suite of water variables covering both water availability and demand. And all of them are found to be relevant, even though partly in different regions. Including several water-related variables allows us to acknowledge the differences in trends of the individual water-related variables, to detect regions and time periods where most water-related variables agree on drying, and to analyse to which extent models acknowledge the influence of this diversity of water-related variables. Also, the regression-based analysis suggests that different water-related variables are relevant for LAI dynamics in different regions such that ignoring their variety would lead to biased results. Another novel aspect of the regression-based analysis is the joint consideration of the role of means and extremes of soil moisture and temperature for LAI dynamics which showed that means are overall more relevant while extremes matter locally.

In addition to the direct effects of water-related variables on greenness, vegetation changes can also feed back into the climate system and the water cycle in particular. For example, reduced plant transpiration as a response to water stress translates into changes in runoff (W. Li et al. 2023) and precipitation (Hoek van Dijke et al. 2022). Vegetation growth leads to decreased terrestrial water storage in drylands (K. Liu et al. 2023), and vegetation greening leads to an increased ratio of transpiration-to-evaporation such that surface energy and water fluxes become more controlled by vegetation (Forzieri et al. 2020). Furthermore, greenness influences surface albedo, which is key for the energy balance of the Earth and thereby influences climate (Forzieri et al. 2017, Duveiller et al. 2018, Y. Li et al. 2023). Other studies show that vegetation affects climate sensitivity, i.e. the response of global mean temperature to increasing atmospheric CO_2 (Zarakas et al. 2020, He et al. 2022).

We consistently perform the analyses in this study for both observation-based data and Earth system model outputs, enabling direct comparison. Earth system models generally capture the relevance of water-related variables for inter-annual greenness dynamics. At the same time we identify some disagreements between observation-based and model-based results that can inform model development. Specifically, models tend to (i) overestimate the influence of water demand on inter-annual greenness dynamics, (ii) underestimate global greening during 1982–2001, even though observation-based trends are uncertain due to temporal inconsistencies in the underlying satellite data (Jeong et al. 2024), (iii) underestimate the diversity of influential water-related variables across different regions, and (iv) show large variation across individual models such that individual models typically agree less well with observation-based findings than the multi-model mean. This way, a promising avenue for model development is to improve the representation of plant hydraulics, including water stress formulations determining the response of stomatal conductance to variations in soil moisture and atmospheric water demand (e.g. Migliavacca et al. 2021). Such development can in turn help to decrease the considerable spread across models and their future projections. Thereby, accurately capturing the effects of water-related variables on vegetation trends can provide more precise information for managing water resources and ecosystems under global change.

Methods

Observation-based data

The water-related variables are sourced from independent datasets; soil moisture is from GLEAMv4.1 (Miralles et al. 2024), precipitation from MSWEP v2.8 (Beck et al. 2019), and VPD from ERA5 (Hersbach et al. 2020). Note, however, that GLEAM is forced with MSWEP precipitation data. Meteorological data (temperature, shortwave radiation and net radiation) are also from ERA5. While ERA5 does not include inter-annual dynamics nor trends in greenness, they are deemed suitable for our analysis thanks to its comprehensive data assimilation across many quantities which can compensate for some model shortcomings. Dryness index is calculated as the ratio between net radiation from ERA5 and unit-adjusted precipitation from MSWEP. Annual means are used for all observation-based data. For LAI, the state-of-the-art GEOV2 dataset was selected as it is a global LAI dataset that is consistent in terms of explicitly reconciling the effects of satellite changes during the time period 1982-recent (Verger et al. 2020). As such, it is less likely to suffer from artifacts due to changes in instrumentation, which have proven to jeopardize interpretation of greenness over long time scales. Note that the last two years of the considered GEOV2 record, 2019–2020, have been reported to be of lower quality (Verger 2023). In addition, for the more recent considered time period 2002–2020 we also use LAI data from MODIS (MOD15A2H.061, Myneni et al. 2021). All employed variables are used on 0.5^{o}x0.5^{o} resolution.

Earth system model output

The same hydrological, meteorological and LAI variables as in the observation-based analysis are considered in the model-based analysis. Earth system models considered here include ACCESS-ESM1-5, CMCC-ESM2, CNRM-ESM2-1, EC-Earth3-CC, GFDL-CM4, MPI-ESM1-2-HR, MPI-ESM1-2-LR, MRI-ESM2-0, and UKESM1-0-LL. We use data from these nine Earth system models because (i) all variables required for this analysis are provided, and (ii) the models do not prescribe LAI but actually simulate it. All models account for land use change through e.g. crop expansion, pasture development, and wood harvest in the historical simulations. Similar to the observational analysis, annual means are used. Root-zone soil moisture is computed as an average of soil moisture per soil layer weighted by the model-dependent thickness of the respective layer between 0-100cm. All employed variables are aggregated temporally to monthly and spatially to 2^{o}x2^{o} resolution.

Trend calculation and related assessment of statistical significance

Trends are calculated by subtracting the mean of the first half of the considered time period from the mean of the second half. Statistical significance of increases or decreases of considered variables in considered time periods is determined through bootstrapping. For this purpose, the difference of the mean values of the first and second half of the considered time period is compared with differences from 300 randomly drawn groups of two samples of the same number of values as the first and second

half of the time period. If the difference between the values of the first and second half of the time period is larger than the 95th percentile or smaller than the 5th percentile of the differences from the randomly drawn samples, it is considered significant.

Regression analysis

We evaluate the effectiveness of various predictors to reproduce inter-annual variations in Leaf Area Index (LAI). The predictors include annual averages of soil moisture, precipitation, vapor pressure deficit, shortwave incoming radiation, net radiation, and temperature, along with annual minima of monthly soil moisture and daily maxima of temperature. Monthly and daily time scales are used here in order to mimic the typical time scales of droughts and heat waves, respectively. The predictors are normalized to range between 0 and 1. A multivariate linear regression approach is employed, utilizing the dredge function from the MuMin package (Burnham & Anderson, 2004; Barton, 2024), similar to the methodology used by Fernández-Martínez et al. (2020) and Denissen et al. (2022). This function tests all possible combinations of predictors and ranks them based on the Akaike Information Criterion (AIC), allowing us to identify a set of models that balance both performance (likelihood) and complexity (number of parameters).

We select models whose AIC difference from the top-ranked model is less than 2, yielding one or more similarly performing models per grid cell. Only models with satisfactory predictive power (adjusted $R^2 > 0.36$) are included in the attribution analysis. If only one model with a single predictor exists, this predictor is considered the most important for that grid cell. When a multivariate model contains multiple predictors, the most influential variable is determined using the variance explained by each predictor, calculated with the 'lmg' metric in the relaimpo R package (Groemping, 2007). In cases with multiple multivariate models, the most important predictor is chosen based on the average variance explained across all models, weighted by the Akaike weights.

Declarations

Acknowledgments

We thank the respective climate modeling groups for making their model output available within the Coupled Model Intercomparison Project Phase 6 (CMIP6) ensemble. We are furthermore thankful to Sujan Koirala (Max Planck Institute for Biogeochemistry) for developing the scripts to download CMIP6 data from Google cloud, as well as Ulrich Weber (Max Planck Institute for Biogeochemistry) and Hao Huang (University of Freiburg, Southern University of Science and Technology) for downloading and aggregating the observation-based data used in this study. We appreciate helpful discussions on the manuscript with Alexander Winkler and Gregory Duveiller (both from Max Planck Institute for Biogeochemistry).

R.O., J.K. and A.H.v.D. acknowledge funding by the German Research Foundation (Emmy Noether grant number 391059971). Further, G.D., A.W., X.Y. and C.Z. acknowledge funding by the European Research Council (Synergy grant number 855187), S. O acknowledges funding by the Basic Science Research Program through the National Research Foundation of Korea (RS-2023-00248706), A.F.F. was supported by a NASA ECOSTRESS grant and NASA Terrestrial Ecology scoping study for a dryland field campaign, and L.W.-E. was supported by funding from Formas (grant numbers 2022-02089, 2023-00321, 2023-00310), the IKEA foundation, and Horizon Europe (grant number 101081661).

References

1. Hersbach et al. 2020, doi: 10.1002/qj.3803, https://rmets.onlinelibrary.wiley.com/doi/10.1002/qj.3803
2. Munoz-Sabater 2019, doi: 10.24381/cds.e2161bac, https://doi.org/10.24381/cds.e2161bac
3. Myneni et al. 2021, doi: 10.5067/MODIS/MOD15A2H.061, https://doi.org/10.5067/MODIS/MOD15A2H.061
4. Barton 2024, https://cran.r-project.org/web/packages/MuMIn/MuMIn.pdf
5. Burnham and Anderson 2004, doi: 10.1177/0049124104268644, https://journals.sagepub.com/doi/10.1177/0049124104268644
6. Fernandez-Martinez et al. 2020, doi: 10.1111/gcb.15385, https://onlinelibrary.wiley.com/doi/10.1111/gcb.15385
7. Groemping 2007, doi: 10.18637/jss.v017.i01, https://www.jstatsoft.org/article/view/v017i01
8. Papagiannopoulou et al. 2017, doi: 10.1088/1748-9326/aa7145, https://iopscience.iop.org/article/10.1088/1748-9326/aa7145
9. K. Liu et al. 2023, doi: 10.1038/s41612-023-00437-9, https://www.nature.com/articles/s41612-023-00437-9
10. Denissen et al. 2022, doi: 10.1038/s41558-022-01403-8, https://doi.org/10.1038/s41558-022-01403-8
11. Li et al. 2022, doi: 10.1038/s41467-022-31667-9, https://doi.org/10.1038/s41467-022-31667-9
12. Zhan et al. 2022, doi: 10.1111/gcb.16397, https://onlinelibrary.wiley.com/doi/epdf/10.1111/gcb.16397
13. Kroll et al. 2022, doi: 10.5194 /bg-19-477-2022, https://bg.copernicus.org/articles/19/477/2022
14. Gulev et al. 2021, doi: 10.1017/9781009157896.004, https://doi.org/10.1017/9781009157896.004
15. Reichstein et al. 2013, doi: 10.1038/nature12350, https://www.nature.com/articles/nature12350
16. Smith et al. 2023, doi: 10.1038/s41586-022-05690-1, https://doi.org/10.1038/s41586-022-05690-1

17. Denissen et al. 2020, doi: 10.1029/2019JD031672, https://doi.org/10.1029/2019JD031672
18. Piao et al. 2019, doi: 10.1111/gcb.14884, https://doi.org/10.1111/gcb.14884
19. Duveiller et al. 2018, doi: 10.1038/s41467-017-02810-8, https://www.nature.com/articles/s41467-017-02810-8
20. Hoek van Dijke et al. 2022, doi: 10.1038/s41561-022-00935-0, https://www.nature.com/articles/s41561-022-00935-0
21. Forzieri et al. 2017, doi: 10.1126/science.aal1727, https://doi.org/10.1126/science.aal1727
22. Ukkola et al. 2016, doi: 10.1038/nclimate2831, https://doi.org/10.1038/nclimate2831
23. Zhu et al. 2016, doi: 10.1038/nclimate3004, https://doi.org/10.1038/nclimate3004
24. Chen et al. 2019, doi: 10.1038/s41893-019-0220-7, https://doi.org/10.1038/s41893-019-0220-7
25. Winkler et al. 2021, doi: 10.5194 /bg-18-4985-2021, https://bg.copernicus.org/articles/18/4985/2021/
26. Ruehr et al. 2023, doi: 10.1038/s43017-023-00456-3, https://www.nature.com/articles/s43017-023-00456-3
27. Bonan et al. 2008, doi: 10.1126/science.1155121, https://doi.org/10.1126/science.1155121
28. Friedlingstein et al. 2022, doi: 10.5194 /essd-14-4811-2022, https://essd.copernicus.org/articles/14/4811/2022/
29. Walker et al. 2021, doi: 10.1111/nph.16866, https://doi.org/10.1111/nph.16866
30. Liu et al. 2021, doi: 10.1016/j.agrformet.2021.108663, https://doi.org/10.1016/j.agrformet.2021.108663
31. Jiao et al. 2021, doi: 10.1038/s41467-021-24016-9, https://www.nature.com/articles/s41467-021-24016-9
32. Seneviratne et al. 2010, doi: 10.1016/j.earscirev.2010.02.004, https://www.sciencedirect.com/science/article/pii/S0012825210000139
33. De Kauwe et al. 2021, doi: 10.1111/nph.17540, https://nph.onlinelibrary.wiley.com/doi/full/10.1111/nph.17540
34. Forzieri et al. 2020, doi: 10.1038/s41558-020-0717-0, https://www.nature.com/articles/s41558-020-0717-0
35. Z. Liu et al. 2023, doi: 10.1088/1748-9326/accfb1, https://iopscience.iop.org/article/10.1088/1748-9326/accfb1
36. Brodribb et al. 2020, doi: 10.1126/science.aat7631, https://www.science.org/doi/10.1126/science.aat7631
37. Seneviratne et al. 2021, doi: 10.1017/9781009157896.013, https://doi.org/10.1017/9781009157896.013

38. Carvalho et al. 2019, doi: 10.1016/j.apgeog.2019.03.001, https://doi.org/10.1016/j.apgeog.2019.03.001
39. Piao et al. 2020, doi: 10.1038/s43017-019-0001-x, https://doi.org/10.1038/s43017-019-0001-x
40. O et al. 2020, doi: 10.1038/s41598-020-67530-4, https://www.nature.com/articles/s41598-020-67530-4
41. W. Li et al. 2023, doi: 10.1029/2022EF003441, https://doi.org/10.1029/2022EF003441
42. Q. Liu et al. 2023, doi: 10.1016/j.tplants.2023.03.024, https://doi.org/10.1016/j.tplants.2023.03.024
43. Zhang et al. 2020, doi: 10.1073/pnas.1914436117, https://www.pnas.org/doi/10.1073/pnas.1914436117
44. Zhang et al. 2022, doi: 10.1038/s41467-022-32631-3 https://doi.org/10.1038/s41467-022-32631-3
45. Forzieri et al. 2022, doi: 10.1038/s41586-022-04959-9, https://www.nature.com/articles/s41586-022-04959-9
46. Liu et al. 2020, doi: 10.1038/s41467-020-18631-1, https://www.nature.com/articles/s41467-020-18631-1
47. Zarakas et al. 2020, doi: 10.1175/JCLI-D-20-0078.1, https://journals.ametsoc.org/view/journals/clim/33/19/jcliD200078.xml
48. Xu et al. 2022, doi: 10.1038/s41467-022-28161-7, https://doi.org/10.1038/s41467-022-28161-7
49. Ruijsch et al. 2023, doi: 10.1088/1748-9326/acd395, https://iopscience.iop.org/article/10.1088/1748-9326/acd395
50. Cheng et al. 2017, doi: 10.1038/s41467-017-00114-5, https://www.nature.com/articles/s41467-017-00114-5
51. Y. Li et al. 2023, doi: 10.1038/s41467-023-35799-4, https://www.nature.com/articles/s41467-023-35799-4
52. Frankenberg et al. 2021, doi: 10.1126/science.abg2947, https://www.science.org/doi/10.1126/science.abg2947
53. Fu et al. 2021, doi: 10.1111/gcb.16050, https://onlinelibrary.wiley.com/doi/abs/10.1111/gcb.16050
54. Gonsamo et al. 2021, doi: 10.1111/gcb.15658, https://onlinelibrary.wiley.com/doi/abs/10.1111/gcb.15658
55. Feldman et al. 2022, doi: 10.1029/2021WR030316, https://agupubs.onlinelibrary.wiley.com/doi/full/10.1029/2021WR030316
56. Anderegg et al. 2020, doi: 10.1038/s41558-020-00919-1, https://www.nature.com/articles/s41558-020-00919-1
57. Huang et al. 2016, doi: 10.1038/nclimate2837, https://www.nature.com/articles/nclimate2837
58. Singh et al. 2022, doi: 10.1111/gcb.16115, https://onlinelibrary.wiley.com/doi/full/10.1111/gcb.16115

59. Lian et al. 2021, doi: 10.1038/s43017-021-00144-0, https://www.nature.com/articles/s43017-021-00144-0
60. He et al. 2022, doi: 10.1038/s43247-022-00489-4, https://www.nature.com/articles/s43247-022-00489-4
61. Vicente-Serrano et al. 2022a, doi: 10.1016/j.earscirev.2022.104055, https://www.sciencedirect.com/science/article/pii/S0012825222001398
62. Anderegg et al. 2015, doi: 10.1126/science.aab1833, https://www.science.org/doi/10.1126/science.aab1833
63. Ruehr et al. 2019, doi: 10.1093/treephys/tpz032, https://academic.oup.com/treephys/article/39/8/1285/5423350
64. de Brito 2021, doi: 10.1016/j.scitotenv.2021.146236, https://www.sciencedirect.com/science/article/pii/S0048969721013048
65. Fan et al. 2017, doi: 10.1073/pnas.1712381114, https://www.pnas.org/doi/full/10.1073/pnas.1712381114
66. Migliavacca et al. 2021, doi: 10.1038/s41586-021-03939-9, https://www.nature.com/articles/s41586-021-03939-9
67. Schumacher et al. 2019, doi: 10.1038/s41561-019-0431-6, https://www.nature.com/articles/s41561-019-0431-6
68. Schumacher et al. 2022, doi: 10.1038/s41561-022-00912-7, https://www.nature.com/articles/s41561-022-00912-7
69. Budyko 1974, https://www.sciencedirect.com/bookseries/international-geophysics/vol/18
70. Donohue et al. 2013, doi: 10.1002/grl.50563, https://agupubs.onlinelibrary.wiley.com/doi/full/10.1002/grl.50563
71. Fu et al. 2022, doi: 10.1038/s41467-022-28652-7, https://www.nature.com/articles/s41467-022-28652-7
72. Vicente-Serrano et al. 2022b, doi: 10.1098/rsta.2021.0285, https://royalsocietypublishing.org/doi/full/10.1098/rsta.2021.0285
73. Verger et al. 2020 https://www.theia-land.fr/wp-content/uploads/2022/03/THEIA-SP-44-0207-CREAF_I2.50-1.pdf
74. Allen et al. 2015, doi: 10.1890/ES15-00203.1, https://esajournals.onlinelibrary.wiley.com/doi/10.1890/ES15-00203.1
75. Stocker et al. 2023, doi: 10.1038/s41561-023-01125-2, https://www.nature.com/articles/s41561-023-01125-2
76. Gentine et al. 2019, doi: 10.1088/1748-9326/ab22d6, https://iopscience.iop.org/article/10.1088/1748-9326/ab22d6
77. Feng et al. 2021, doi: 10.1016/j.scib.2021.02.023, https://www.sciencedirect.com/science/article/abs/pii/S209592732100164X

78. Novick et al. 2016, doi: 10.1038/nclimate3114, https://www.nature.com/articles/nclimate3114
79. Wang et al. 2022, doi: 10.1038/s41558-022-01499-y, https://www.nature.com/articles/s41558-022-01499-y
80. Jiang et al. 2017, doi: 10.1111/gcb.13787, https://onlinelibrary.wiley.com/doi/10.1111/gcb.13787
81. Yang et al. 2023, doi: 10.1038/s43017-023-00464-3, https://www.nature.com/articles/s43017-023-00464-3
82. He et al. 2023, doi: 10.1016/j.scitotenv.2022.159942, https://www.sciencedirect.com/science/article/abs/pii/S0048969722070425
83. Chen et al. 2019, doi: 10.1038/s41893-019-0220-7, https://www.nature.com/articles/s41893-019-0220-7
84. Li et al. 2024, doi: 10.1038/s43017-024-00543-z, https://www.nature.com/articles/s43017-024-00543-z
85. Jeong et al. 2024, doi: 10.1016/j.rse.2024.114282, https://www.sciencedirect.com/science/article/pii/S0034425724003006
86. Miralles et al. 2024, GLEAM4: global evaporation and soil moisture datasets at 0.1° resolution from 1980 to near present, *in prep*.
87. Beck et al. 2019, doi: 10.1175/BAMS-D-17-0138.1, https://journals.ametsoc.org/view/journals/bams/100/3/bams-d-17-0138.1.xml
88. Verger 2023 https://www.theia-land.fr/wp-content/uploads/2018/12/THEIA-QAR-RP-44-0281-CSIC_I2.0.pdf

Figures

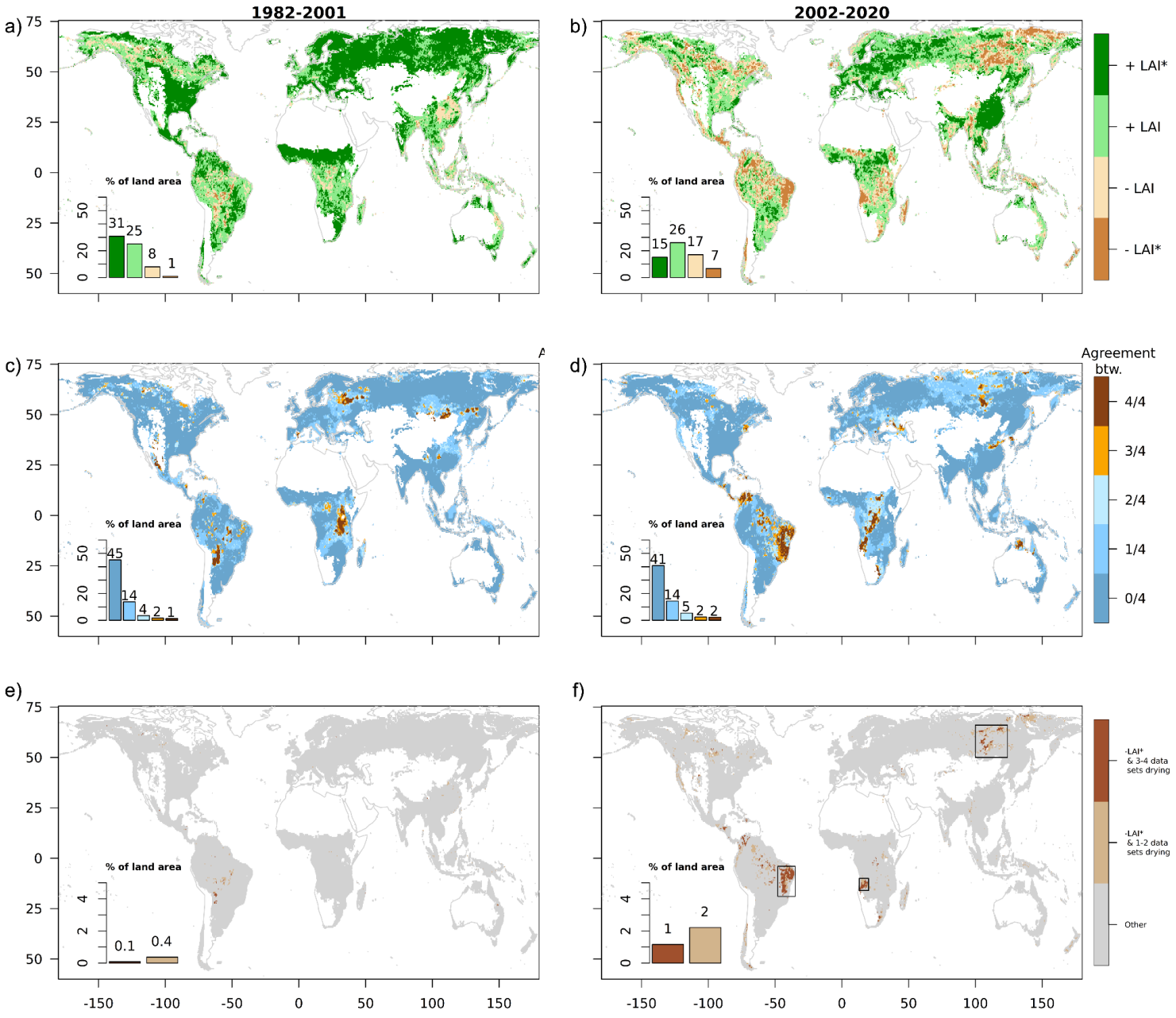

Figure 1

Observation-based trends in leaf area index (LAI) and water variables during 1982–2001 (left) and 2002–2020 (right).(a-b) Trends of LAI based on GEOV2. Significant trends at the 95% confidence level are marked with asterisks (see Methods). (c-d) Number of water-related variables that show drying trends, defined as decreasing water availability or increasing water demand; variables considered are root-zone soil moisture, precipitation, vapor pressure deficit and dryness index (calculated as the ratio between net radiation and precipitation). (e-f) Regions of coinciding browning and drying trends. Boxes in panel (f) denote focus regions. All trends are determined as the difference between the two considered decades. White areas denote regions where the decadal mean LAI is below 0.5 in any of the four considered decades.

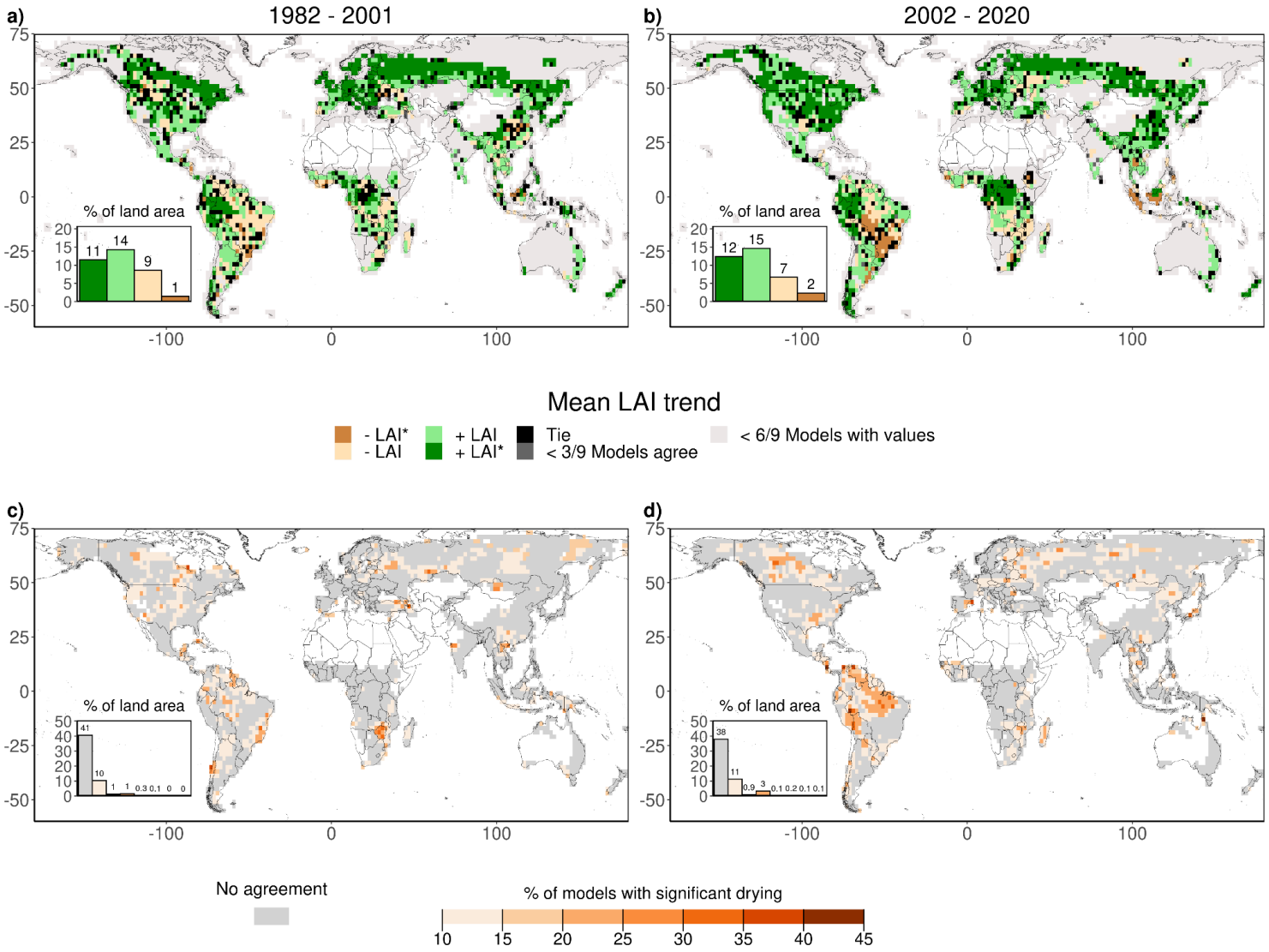

Figure 2

Model-based trends in leaf area index (LAI) and water variables during 1982–2001 (left) and 2002–2021 (right). Analysis is performed for each of nine Earth system models separately and the figure shows summarized results. (a,b) Trends in LAI. Coloring of each grid cell indicates the most frequently occuring trend category (significant/insignificant greening or browning) across the model ensemble. Significance trends at the 95% level are marked with asterisks (see methods). Gray colors indicate limited model data availability or low agreement between models. Black color denotes that more than one trend category is most occurring across the same number of models. (c,d) Fraction of models simulating significant drying for at least two variables. Drying is quantified through decreasing water availability or increasing water demand; variables considered are root-zone soil moisture, precipitation, vapour pressure deficit and dryness index. Analyses are restricted to grid cells with data from at least five models. All trends are determined as the difference between the two considered decades.

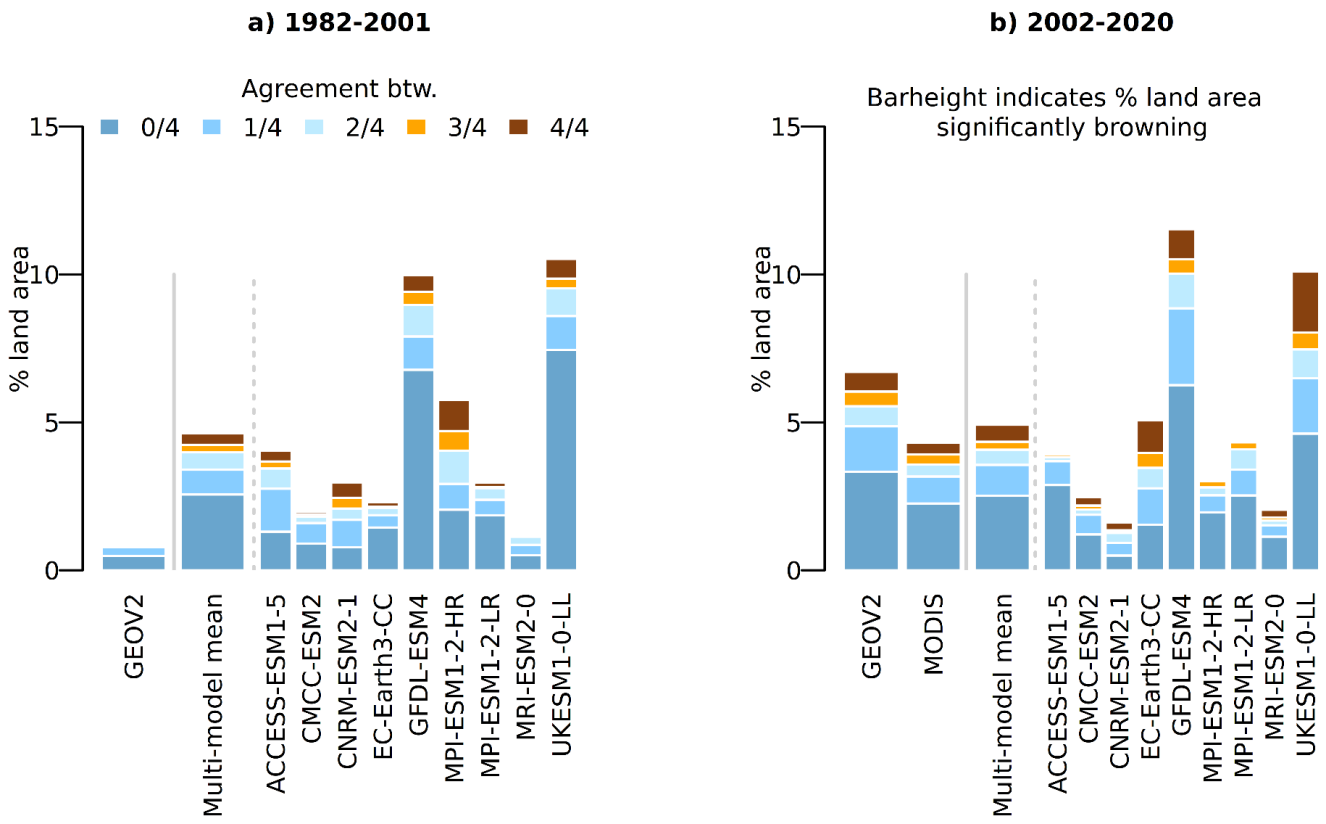

Figure 3

Degree of drying in areas of significant browning in observations and models during (a) 1982–2001 and (b) 2002–2021. Height of bars indicates the size of the area with significant browning. Bar colors denote the agreement of water-related datasets on drying, quantified by decreasing water availability or increasing water demand; variables considered are root-zone soil moisture, precipitation, vapour pressure deficit and dryness index. Observation-based results from MODIS shown for 2002-2020 period only due to limited data availability. Multi-model mean is calculated as the average across results from individual models.

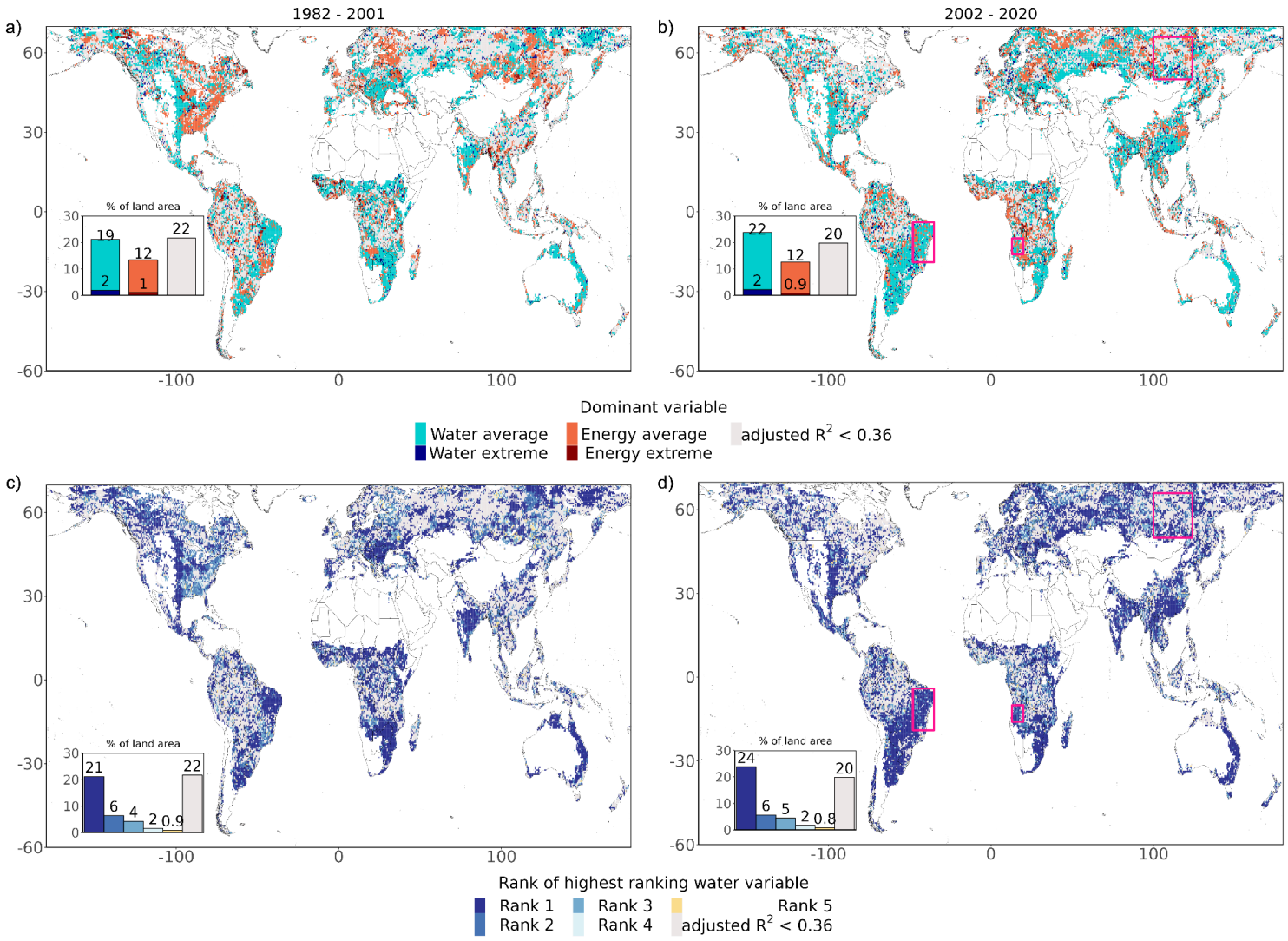

Figure 4

Observation-based assessment of drivers of inter-annual LAI dynamics during 1982-2001 and 2002-2020. (a-b) Dominant variable as determined in regression-based analysis (see Methods). Turquoise color indicates a water variable (i.e. mean soil moisture, precipitation, or vapour pressure deficit) as the strongest driver, while red color indicates an energy variable (i.e. mean temperature, net radiation, or incoming short-wave radiation). Dark blue and dark red denote extremes in soil moisture and temperature, respectively. (c-d) Rank of the highest-ranked water variable in the regression-based analysis. Boxes in panels b and d denote focus regions identified in Figure 1.

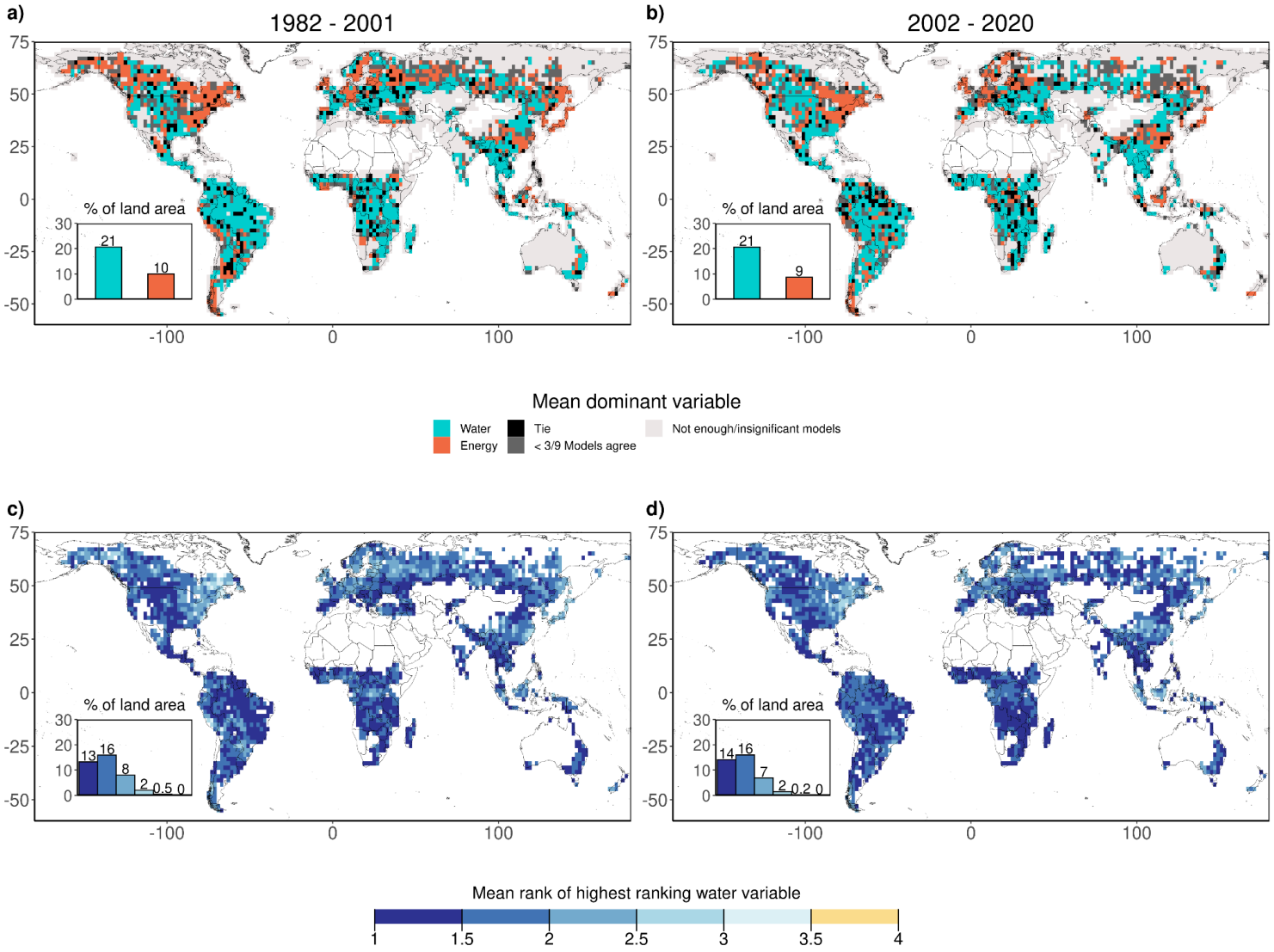

Figure 5

Model-based assessment of drivers of inter-annual LAI dynamics during 1982-2001 and 2002-2020. Analysis is performed for each of nine Earth system models separately and the figure shows summarized results. (a-b) Dominant variable as determined in regression-based analysis (see Methods). Turquoise color indicates a water variable (i.e. mean soil moisture, minimum soil moisture, precipitation, or vapour pressure deficit) as the strongest driver, while red color indicates an energy variable (i.e. mean temperature, maximum temperature, net radiation, or short-wave radiation). Dark gray color indicates that less than three models agree on the most-occuring trend category. Black color denotes that different trend categories are most-occurring across the same number of models (denoted as Tie). (c-d) Mean rank of the highest-ranked water variable across models in the regression-based analysis.

Supplementary Files

This is a list of supplementary files associated with this preprint. Click to download.

- Supplement.pdf